OFFICE OF NAVAL RESEARCH

Contract N00014-85-K-0474

Technical Report No. 18

Determination of Ion Power Density During Reactive-Ion Etching from Temperature Measurements Using Laser Interferometry

by

B. C. Dems and F. Rodriguez

Presented in part before the
Annual Meeting of the American Institute of Chemical
Engineers,San Francisco, CA, Nov. 5-10, 1989

Olin Hall, Cornell University
School of Chemical Engineering
Ithaca, NY 14853

May 7, 1990

SECURITY CLASSIFICATION OF THIS PAGE

REPORT DOCUMENTATION PAGE

Form Approved OMB No. 0704-0188

1a. REPORT SECURITY CLASSIFICATION: Unclassified	1b. RESTRICTIVE MARKINGS
2a. SECURITY CLASSIFICATION AUTHORITY	3. DISTRIBUTION/AVAILABILITY OF REPORT: Approved for public release. Distribution is unlimited.
2b. DECLASSIFICATION/DOWNGRADING SCHEDULE	
4. PERFORMING ORGANIZATION REPORT NUMBER(S): Technical Report No. 18	5. MONITORING ORGANIZATION REPORT NUMBER(S)
6a. NAME OF PERFORMING ORGANIZATION: Cornell University; 6b. OFFICE SYMBOL (If applicable)	7a. NAME OF MONITORING ORGANIZATION: Office of Naval Research
6c. ADDRESS (City, State, and ZIP Code): Olin Hall, Cornell University, Ithaca, NY 14853	7b. ADDRESS (City, State, and ZIP Code): 800 North Quincy Street, Arlington, VA 22217
8a. NAME OF FUNDING/SPONSORING ORGANIZATION: Office of Naval Research; 8b. OFFICE SYMBOL (If applicable)	9. PROCUREMENT INSTRUMENT IDENTIFICATION NUMBER: N 00014-85-K-0474
8c. ADDRESS (City, State, and ZIP Code)	10. SOURCE OF FUNDING NUMBERS: PROGRAM ELEMENT NO. / PROJECT NO. / TASK NO. / WORK UNIT ACCESSION NO.

11. TITLE (Include Security Classification): Determination of Ion Power Density During Reactive-Ion Etching from Temperature Measurements Using Laser Interferometry

12. PERSONAL AUTHOR(S): B. C. Dems and F. Rodriguez

13a. TYPE OF REPORT	13b. TIME COVERED	14. DATE OF REPORT (Year, Month, Day)	15. PAGE COUNT
Technical Report	FROM _____ TO _____	90 May 7	28

16. SUPPLEMENTARY NOTATION: Presented in part at the Annual Meeting of the Amer. Inst. of Chem. Engineers, San Francisco, Nov. 5-10, 1989

17. COSATI CODES		
FIELD	GROUP	SUB-GROUP

18. SUBJECT TERMS (Continue on reverse if necessary and identify by block number): Reactive-Ion Etching, Ion Power Density, Ion Energy Flux, Laser Interferometry, Resist, PMMA, PLASMAS(PHYSICS), POLYMERS (JG)

19. ABSTRACT (Continue on reverse if necessary and identify by block number): reactive-ion etching

A method to determine the ion power density during RIE using a laser interferometer is described. Thickness changes due to heating of thin (< 0.3 cm) plate-glass substrates during RIE processing are monitored via interferometry. The thickness changes are directly related to temperature changes within the isothermal substrate, which allows the plate-glass temperature to be monitored accurately and non-intrusively. Ion energy flux determinations follow directly from the heating and cooling dynamics of the substrate. The measured ion energy fluxes are constant for all times during a run to within experimental error (±10%) and are in good agreement with predictions given by the space-charge limited flux expression. The rf power transfer efficiency, defined as the ion energy flux delivered to the cathode relative to the nominal rf input power, is less than 30%. The O_2 RIE rate of poly(methyl methacrylate) and polystyrene were found to vary linearly with the measured ion energy flux to the surface over a broad range of processing conditions.

(6K-1987)

20. DISTRIBUTION/AVAILABILITY OF ABSTRACT: ☒ UNCLASSIFIED/UNLIMITED ☐ SAME AS RPT ☐ DTIC USERS	21. ABSTRACT SECURITY CLASSIFICATION: Unclassified
22a. NAME OF RESPONSIBLE INDIVIDUAL: Dr. J. Milliken	22b. TELEPHONE (Include Area Code): (202) 696-4410; 22c. OFFICE SYMBOL

DD Form 1473, JUN 86 — Previous editions are obsolete. — SECURITY CLASSIFICATION OF THIS PAGE

Determination of Ion Power Density During Reactive-Ion Etching from Temperature Measurements Using Laser Interferometry

B.C. Dems and F. Rodriguez, School of Chemical Engineering
Cornell University, Ithaca, New York 14853

A method to determine the ion power density during RIE using a laser interferometer is described. Thickness changes due to heating of thin ($d < 0.3$ cm) plate-glass substrates during RIE processing are monitored via interferometry. The thickness changes are directly related to temperature changes within the isothermal substrate, which allows the plate-glass temperature to be monitored accurately and non-intrusively. Ion energy flux determinations follow directly from the heating and cooling dynamics of the substrate. The measured ion energy fluxes are constant for all time during a run to within experimental error (±10%) and are in good agreement with predictions given by the space-charge limited flux expression. The rf power transfer efficiency, defined as the ion energy flux delivered to the cathode relative to the nominal rf input power, is less than 50%. The O_2 RIE rate of poly(methyl methacrylate) and poly(styrene) were found to vary linearly with the measured ion energy flux to the surface over a broad range of processing conditions.

INTRODUCTION

Reactive-ion etching (RIE) is a plasma process commonly used to produce highly anisotropic circuit features in the fabrication of very large scale integrated (VLSI) circuits. However, the fundamental plasma-surface interactions, which govern the etching process, are not well understood. These shortcomings will eventually limit the usefulness of RIE technology in future generations of chip-making processes, unless further improvements in these areas can be made.

Recent studies of the oxygen reactive-ion etching of organic polymer resist materials have revealed that the ion energy flux to the powered-electrode (cathode) surface appears to be the principal controlling factor

---

Presented in part at the Annual Meeting of AIChE, San Francisco, November 5 - 10, 1989.

of etch rate [1,2]. In addition, the ion energy flux, or ion power density, to the cathode surface is intimately related to substrate temperature dynamics. Large variations in substrate temperature can drastically affect etch rate leading to an overall decrease in process controllability. Thus, it is essential to quantify the relationship between ion energy flux and etch rate over a wide range of processing conditions. This necessitates the further development and implementation of accurate and reliable measurement techniques.

Determination of Ion Power Density

The ion power density to the electrodes during radio-frequency (rf) plasma processes, as pointed out by Visser [3], is not easily obtained. One way to determine ion power density is by measuring the ion current density (ion flux) and the dc self-bias potential independently, and then multiplying the two together, which yields the ion power density. A Faraday-cup in conjunction with a picoammeter can be used to measure the ion current density at the cathode. However, rf applications of conventional current-voltage probe techniques are unreliable, since the finite parasitic capacitance and inductance properties of the connecting wires can alter the current-voltage characteristics of the probe significantly [4].

Visser has shown that substrate heating during RIE processing is due, almost exclusively, to high-energy ion bombardment. By performing an elementary energy balance on the substrate, he showed that the ion power density, q_+, can be determined directly from <u>in situ</u> substrate temperature measurements [4].

Substrate Temperature Measurement Devices

For his study, Visser used a fluoroptic probe to measure the temperature dynamics of a silicon wafer immersed in the RIE reactor. Fluoroptic

probes are very accurate and well-suited for rf applications, but they are also expensive and require a highly undesirable external connection between the wafer and the outside of the apparatus.

It was of interest in this work to see if a less expensive, possibly simpler, technique could be developed to measure substrate temperature (and therefore q_+) during RIE processing. Several alternative substrate temperature sensing devices were available, which included: conventional thermocouple junctions that have been shielded or removed from the plasma [5,6], infrared pyrometry, and laser interferometry.

Junction thermocouples, like any other electrical measurement scheme at rf frequencies, are vulnerable to signal interference effects due to stray inductance effects. Infrared thermometers, designed specifically for silicon wafer applications, are sensitive only to temperatures above about 200°C [7]. However, laser interferometry can been used to monitor accurately the rate of thermal expansion of optically smooth plate-glass substrates immersed in a plasma reactor [8]. By relating the rate of thermal expansion to the rate of substrate temperature rise, substrate temperature is measured accurately and non-intrusively (i.e. no external electrical connections are required).

Laser Interferometer Thermometer

Since the RIE system in our laboratory was already equipped with a laser interferometer, this method was chosen to make <u>in situ</u> substrate temperature measurements. At the very least, this technique could be used as a comparative tool to measure differences in rates of heating and cooling and steady-state temperatures as the RIE processing conditions were changed.

It turned out to be a much more powerful tool, enabling ion energy heat fluxes to be determined absolutely.

In order to incorporate a laser interferometer plate-glass thermometer into a system, certain conditions must be satisfied. They include: constant plate-glass physical properties; thermal expansion rate >> material removal rate by sputtering and/or chemical etching; and negligible thermal gradients within the sample.

These conditions are not constraining, at least for the case of argon and oxygen plasma environments, used initially in this study. The physical properties that are most critical to the operation of the plate-glass laser interferometer, namely, specific heat, mass density, and coefficient of linear thermal expansion, are generally constant in the 0 to 400°C range for a multitude of $Na_2O \cdot SiO_2$ glasses [9].

Thermal expansion rates are on the order of 500 nm/min, which is at least an order of magnitude greater than sputtering rates of SiO_2 by hundred keV ions [10]. Finally, heat fluxes during RIE processes, estimated from the space-charge-limited ion current, are approximately an order of magnitude less than thermal conductive heat fluxes within a plate-glass substrate. This implies that for the case of substrate heating during RIE processing, thermal gradients within the plate-glass specimen are negligible and can safely be ignored (see appendix for more details).

Theory of Operation

The change in thickness of the plate-glass specimen, Δd, is related to the change in specimen temperature, ΔT_s, by

$$\Delta d = \alpha \cdot d_o \cdot \Delta T_s \qquad (1)$$

where α is the coefficient of thermal expansion and d_o is the initial specimen thickness. When a laser beam of vacuum wavelength λ is aimed obliquely at the plate-glass surface (figure 1), a change in thickness changes the optical path difference between two successive rays measured on a common wavefront. The phase angle, ϕ_2, between the two rays is given by,

$$\phi_2 = 4\pi n_2 d\cos\vartheta_2/\lambda \tag{2}$$

where n_2 is the refractive index of the plate-glass and ϑ_2 is the incident beam angle within the substrate. The ratio of reflected light intensity to incident intensity, R, is a periodic function of glass thickness, all other parameters remaining fixed. The thickness period, d_p, corresponding to the thickness change required for one complete reflectance oscillation to occur, is given by,

$$d_p = \left(\frac{\lambda}{2n_2 [1-(n_1/n_2)^2 \sin^2\vartheta_1]^{1/2}} \right) \tag{3}$$

where n_1 is the plasma refractive index (=1.0). For the case of thermal expansion, d_p is related to a characteristic change in temperature, ΔT_p, given by,

$$\Delta T_p = d_p/(\alpha d_o) \tag{4}$$

which forms the basis for a temperature measurement device. Substituting equation 4 into equation 3,

$$\Delta T_p = \left(\frac{\lambda}{2n_2 \alpha d_o [1-(n_1/n_2)^2 \sin^2\vartheta_1]^{1/2}} \right) \tag{5}$$

The total change in temperature, ΔT_{tot}, follows directly,

$$\Delta T_{tot} = N \cdot \Delta T_p \tag{6}$$

where N is the total number of interference fringes recorded. Measurement resolution is seen to vary inversely with d_o. However, increasing d_o also attenuates the amplitude ratio of the laser waveform, which ultimately limits the ability to resolve local minima/maxima. Experimentally, this turned out to be about d_o=0.3 cm.

One notes that the constant ΔT_p can be determined a priori from a knowledge of a few physical properties. The refractive index of plate-glass can be estimated from the literature to within a few percent. A larger degree of uncertainty lies in the estimate of α, associated with variations in glass composition. Values of α for soda-lime plate-glass reported in the literature range from 9 x 10^{-6} [11] to 16 x 10^{-6} ppm/°C [12,13]. Assuming n_2=1.52, ϑ_1=10°, and d_o= 0.25 cm, a ΔT_p range between 11.0 and 19.7°C/fringe is obtained.

Therefore, unless reliable data are available for the specific grade of plate-glass being used, α should be determined experimentally, or the plate-glass thermometer should be calibrated independently. The plate-glass thermometer calibration methodology and results are given in the appendix.

Ion Energy Flux Determination

Ion energy flux determinations followed directly from the in situ temperature measurements of plate-glass specimens. Since temperature gradients within the specimen were negligible (this will be shown later), a macroscopic energy balance for the plate-glass specimen yielded,

$$(\rho_s C_p d)dT_s/dt = q_n(T_s) = q_+ - q_L(T_s) + q_{rxn}(T_s) \qquad (7)$$

where: $q_n(T_s)$ = net energy (heat) flux
q_+ = ion energy flux
$q_L(T_s)$ = energy flux from the substrate to surroundings

$q_{rxn}(T_s)$ = heat flux due to surface chemical reactions

ρ_s = density

C_p = heat capacity

Photon energy fluxes were neglected since they are typically about three orders of magnitude less than ion energy fluxes during RIE processing [2]. The contribution to energy impingement flux by fast neutral species, for example, those on the high-energy tail of the Maxwellian (assumed) distribution, was also neglected since the concentration of these species is generally very small. The ion energy flux is independent of substrate temperature and originates from the field assisted positive ions, which have diffused to the sheath region and are accelerated across the dark space. For a plasma-to-cathode potential drop of V volts, an average energy of V eV/ion is delivered to the cathode surface.

The laser interferometer thermometer will be most effective as a RIE diagnostic tool when the magnitude of $q_{rxn}(T_s)$ in equation 7 is small relative to q_+. In this case, q_+ is readily determined from equation 7 since $q_n(T_s)$ and $q_L(T_s)$ are directly measurable quantities,

$$q_+ = q_n(T_s) + q_L(T_s) \tag{8}$$

The heat loss function $q_L(T_s)$ is measured from the substrate cooling curve after the plasma has been extinguished ($q_+=0$).

In cases where the gas and substrate interact (i.e. etching of glass with fluorinated gases), substrate temperatures could be significantly higher [14] since q_+ and $q_{rxn}(T_s)$ both contribute to substrate heating. In this case, very little information is gained beyond the temperature-time profile of the plate-glass substrate.

However, preliminary experiments, in which temperature-versus-time profiles for plate-glass specimens were measured using a 92/8 vol.% gas

mixture of CF_4/O_2, were, more or less, the same as those measured in argon. This suggests that the q_{rxn} term in equation 7, even in the case of an etch gas that is reactive towards the plate glass, is negligible (relative to the q_+ term) and can be ignored.

In an oxygen plasma, additional heat generated by recombination between two oxygen atoms ($\Delta H = -33$ kcal/mol) on the plate-glass substrate is a distinct possibility. An upper bound estimate of the heat generation rate due to oxygen atom recombination using kinetic gas theory is on the order of 10^{-1} watt/cm^2, or the same order of magnitude as argon ion energy fluxes during typical RIE conditions.

Experimentally, there was no evidence of additional heat flux by chemical reaction. Measured oxygen ion fluxes tracked closely with (inert) argon fluxes to within experimental error, suggesting a negligible heat generation term in the heat balance. Therefore, all substrate heating was attributed to the ion energy flux.

EXPERIMENTAL

All of the experiments were carried out using a custom-built, asymmetric, parallel-plate reactive-ion etching apparatus described previously [15,16]. A square plate-glass specimen (width = 5.0 cm) was placed in casual contact with the powered electrode. The substrate temperature was allowed to equilibrate with the temperature-controlled electrode (25.0 ± 0.5°C). The He-Ne laser beam was aimed obliquely at the glass substrate (ϑ_1=6°) and reflected off the polished aluminum electrode surface. The reflected intensity was measured with a photodiode and digitally recorded.

Gas flow was introduced and the pressure was throttled to the desired conditions prior to plasma ignition. After igniting the plasma, the substrate

was allowed to heat until a steady-state temperature (constant reflectance) had been reached. Substrate cooling dynamics were then measured by extinguishing the plasma while continuing to monitor the reflected laser intensity.

Heat Flux Measurement

In general, the net heat flux to the substrate, $q_n(T)$, at some average glass substrate temperature, $\overline{T}_s$, is given by $q_n(\overline{T}_s) = \rho_s C_p d(dT_s/dt)$, where ρ_s, C_p, and d are the substrate mass density, specific heat capacity, and thickness ($d \approx d_o$ since $\Delta d/d_o = \alpha \Delta T_{tot} \ll 1$), respectively. The average glass temperature, $\overline{T}_s$, was calculated in the following manner. Letting,

$$T_s(t_n) = \text{Substrate temperature at time } t_n \tag{9a}$$

$$T_s(t_{n+1}) = \text{Substrate temperature at time } t_{n+1} \tag{9b}$$

$\overline{T}_s$ was approximated as,

$$\overline{T}_s \approx [\, T_s(t_n) + T_s(t_{n+1}) \,] / 2 \tag{10}$$

The net heat flux $q_n(\overline{T}_s)$ was then approximated as,

$$q_n(\overline{T}_s) \approx \rho_s C_p d \left(\frac{T_s(t_{n+1}) - T_s(t_n)}{t_{n+1} - t_n} \right) \tag{11}$$

RESULTS AND DISCUSSION

Ion Energy Flux Determination

Typical interferograms obtained during heating and cooling of a 0.237 cm x 5.0 cm x 5.0 cm plate-glass specimen (ΔT_p=7.1°C/fringe) during argon and oxygen RIE are shown in figure 2. The RIE conditions were fixed at 0.50 watt/cm^2 nominal rf input, 35 mTorr pressure, and 20 SCCM (std. cm^3/min) gas flow rate. Temperature versus time plots were constructed from the waveforms

(figures 3a and 3b) so that ion energy fluxes ($-q_+$) could be determined from equation 8.

Ion energy fluxes (figure 4) are seen to be constant to within experimental error ($\pm$ 1$\sigma \approx$10%) throughout the run. Run to run variations were approximately ±10% (Table I).

Table I. Run to run determination of ion energy flux† at a nominal rf power density of 0.50 W/cm^2.

Run	Oxygen	Argon
1	0.112	0.137
2	0.095	0.119
3	0.087	0.120
4	0.102	0.115
5	0.089	0.115
Average	0.096 ± 0.012	0.121 ± 0.009

† RIE Conditions: 20 SCCM Oxygen, 35 mTorr, −600 Vdc, Al cathode

Effect of Nominal Incident Power Density

Temperature-time profiles of plate-glass specimens were measured as a function of nominal incident rf power density in argon and oxygen plasmas (figures 5a and 5b). The pressure and gas flow rate were fixed at 35 mTorr and 20 SCCM gas flow rate, respectively.

Steady-state temperature (figure 6) and ion energy flux (figure 7) increased with increasing rf power density. Energy fluxes were 25 to 40% greater in argon than in oxygen.

The steady-state temperature in argon was correspondingly higher at constant rf power. Note also that the rf power transfer efficiency, defined as the ratio of ion power density (q_+) to nominal input rf power density, is only 20 to 30% (figure 8). This inefficiency is due to a combination of

power loss mechanisms which include: (a) power dissipation occurring on the sides of the cathode assembly which is contacted by the plasma (since the plasma is not confined exclusively between the top cathode surface and the top lid of the chamber); (b) power dissipation through low energy ion bombardment at the anode (grounded surfaces); and (c) resistive heating generated by stray rf currents flowing through the system [1].

These results may explain the difficulty encountered when comparing etch rate data from two different sources at nominally equal processing conditions. The rf power transfer efficiency is not universally predictable and it is likely to vary from system-to-system. Thus, the actual ion energy flux (q_+) to the surface (and RIE rate, since RIE rate tracks closely with q_+) will vary accordingly.

Comparison of Experimental Ion Energy Fluxes With Theory

The ion energy fluxes determined experimentally with the laser interferometer were compared to the collision-free, space-charge-limited energy flux, q_{CF}. The energy flux q_{CF} is equal to the product $J_{CF} \cdot V$, where V is the potential drop across the cathode dark space[1] and J_{CF} is the space-charge-limited ion flux, associated with a collision-free (CF) sheath. An expression for J_{CF} was derived by Child [17] and Langmuir [18],

$$J_{CF} = \left(\frac{4V^{3/2}\epsilon_o}{9S^2} \right) \left(\frac{2}{em_i} \right)^{1/2} \qquad (12)$$

In this expression, S is the optical dark space thickness (measured with a cathetometer in this work), ϵ_o is the vacuum permittivity, e is the charge of an electron, and m_i is the ion mass.

---

[1] For an asymmetrically configured RIE system, V exceeds the measured self-bias potential by only 10 to 20 volts.

Child and Langmuir neglected two main effects in their derivation of equation 12: (a) the contribution of electrons to the space-charge, and (b) inter-sheath ion collisional processes. Neglecting ion collisions within the sheath further implies that the ion energy distribution is monodisperse, and that the mean ion energy is equal to $e\Delta$ electron-volts.

Ion Energy Flux Versus Pressure in Oxygen

The ion energy flux (q_+) was determined as a function of pressure under O_2 RIE conditions (figure 9). The rf power density was varied at three levels (0.25, 0.50, and 0.75 W/cm^2) while the gas flow rate was held constant (20 SCCM O_2). The measured ion energy fluxes (figure 9) were in remarkably good agreement with CF theory predictions. Other workers have reported similar results (different measurement techniques) [2,19], which suggests that the use of q_{CF} yields a good first estimate of the actual ion power density at the cathode.

The largest deviation occurred at 5 mTorr, where the experimental values exceeded CF predictions by about a factor of two. This was surprising since the best agreement between experiment and CF theory was expected at the lowest pressure (5 mTorr), where the probability for ion collisions is the smallest.

It is likely that the discrepancy in the results at 5 mTorr was due to experimental error in the measurement of S. At pressures greater than 15 to 20 mTorr, the plasma-sheath boundary was sufficiently well-defined such that a good estimate of S could be obtained. However, as pressure was reduced below 10 mTorr or so, the plasma-sheath boundary became extremely diffuse in character, making it difficult to measure S accurately. The measured value of S at 5 mTorr was 2.30 cm. If the deviation between experiment and CF

theory was attributed solely to error in the measurement of S, then the true value of S should have been about $2.3/\sqrt{2} = 1.63$, since the ion energy flux is inversely proportional to the square of S.

Relation of q_+ to Polymer Etch Rate

Since ion energy flux (ion power density) appears to be the main determining factor of etch rate during RIE processing, it was important to relate the measured ion energy fluxes to polymer etch rates that were obtained on the same RIE system. To pursue this idea further, oxygen RIE rates of poly(methyl methacrylate) (PMMA) and poly(styrene) (PS) were measured at the same nominal conditions used in the determination of q_+. Three-inch diameter silicon wafers were used as substrates, which were thermally bonded to the quartz cathode surface with a thin film of high-vacuum grease. Etch rates were monitored in the center of the silicon wafers using a laser interferometer. The results are shown in figures 10.

The etch rates of PMMA and PS were a complicated function of pressure and rf power. Oxygen reactive-ion etch rate (ER) was a strong function of pressure in the 5 to 35 mTorr range, where ER approximately doubled for both polymers. As pressure was increased above 35 mTorr, the slope of the curves decreased markedly. For pressures greater than 65 mTorr, the curves for PMMA saturated with pressure (slope ≈ 0), whereas the curves for PS did not saturate, but continued to increase at a slow but measurable rate (0.4 to 1.7 nm/min per mTorr).

Although ER for PMMA and PS was a complex function of pressure and rf power, there was a definite correlation between ER and q_+ (figure 11). The linear dependence of ER on q_+ suggests that the O_2 RIE rate of polymers is

rate-limited by the energy bombardment flux over a relatively broad range of processing conditions. Also plotted in figure 12 are the data obtained by Visser and de Vries [1], who measured q_+ and the O_2 RIE rate of novolac resist, which, like PS, is an aromatic-rich resin. The PS and novolac data overlay and follow the same trend, even though the data were obtained on radically different systems (Visser and de Vries used a nearly symmetric electrode arrangement as opposed to the highly asymmetric system used in this work).

SUMMARY

When plate-glass substrates are subjected to RIE processing conditions, thickness changes are a direct measure of temperature changes. The interferometer monitors these changes continuously and non-intrusively. Cooling curves in the absence of plasma supplement the *heating curves*. An energy balance determines the ion energy flux.

The predictions for ion energy flux using the classical space-charge-limited flux expression of Child and Langmuir agree well with the experimental data under most conditions. Only at the lowest pressure, where measurement of the sheath thickness is difficult, is there a real difference between predicted and experimental values.

ACKNOWLEDGMENTS

This work was supported in part by the Office of Naval Research. Work was performed in cooperation with the National Nanofabrication Facility which is partially supported by the National Science Foundation.

NOMENCLATURE

C_p	specific heat capacity of substrate
d	thickness
d_o	initial specimen thickness
d_p	thickness period
ER	Oxygen reactive-ion etch rate
e	charge of an electron
ΔH	recombination enthalpy
J_{CF}	theoretical ion flux (collision-free sheath)
m_i	ion mass
n_1, n_2	indices of refraction for plasma and substrate, respectively
N	number of interference fringes
q_{CF}	theoretical energy flux (collision-free sheath)
q_+	ion power density, ion energy flux
$q_L(T_s)$	energy flux from substrate to surroundings
$q_n(T_s)$	net energy flux
$q_{rxn}(T_s)$	energy flux due to surface chemical reactions
S	optical dark space thickness
ΔT_p	characteristic change specimen temperature
T_s	substrate temperature
$T_s(t)$	average glass substrate temperature at time t
ΔT_s	change in speciment temperature
ΔT_{tot}	total change in temperature
t	time
V	potential drop across cathode dark space
α	linear coefficient of thermal expansion

λ vacuum wavelength of laser beam

ϵ_o vacuum permittivity

θ_1 incident beam angle through plasma

θ_2 incident beam angle within the substrate

ρ_s density of substrate

ϕ_2 phase angle

REFERENCES

1. R.J. Visser and C.A.M. de Vries, Proceedings 8th International Symp. on Plasma Chemistry, K. Akashi and A. Kinbara (eds.), (IUPAC, Tokyo, 1987), p. 1029.

2. C.W. Jurgensen, in "Polymers in Microlithography," ACS Symp. Ser 412, Washington, D.C. (1989), pp. 210-233.

3. R.J. Visser, J. Vac. Sci Technol. A, 7(2), 189 (1989).

4. W.G.M. van den Hoek, C.A.M. de Vries, and M.G.J. Heijman, J. Vac. Sci. Technol. B, 5(3), 647 (1987).

5. J.M. Cook and B.W. Benson, J. Electrochem. Soc., 130, 2459 (1983).

6. G.N. Taylor and T.M. Wolf, Polym. Eng. Sci., 20(16), 1087 (1980).

7. Infrared Thermometer Brochure, IRCON, Inc., Niles, IL (1988).

8. R.A. Bond, S. Dzioba, and H.M. Naguib, J. Vac. Sci. Technol., 18(2), 335 (1981).

9. O.V. Masurin, M.V. Streltsina, and T.P. Shvaiko-Shvaikovskaya, Handbook of Glass Data, Elsevier Science Publishers, New York (1983).

10. C.W. Jurgensen, S.N. Dudash, E. Reichmanis, and M.J. Vasile, J. Vac. Sci. Technol. A, 6(5), 2938 (1988).

11. "Engineering Materials Handbook," ed. C.L. Mantell, McGraw-Hill, New York (1958), ch. 27.

12. H.F. Shermer, J. Res. Nat. Bur. Stand., 57, 97 (1956).

13. E. Seddon and W.E.S. Turner, J. Soc. Glass Technol., 17, 324 (1933).

14. K.M. Eisele, Rev. Phys. App., 13, 701 (1978).

15. B.C. Dems, F. Rodriguez, C.M. Solbrig, Y.M.N. Namaste, and S.K. Obendorf, Intern. Polymer Processing, 4(3), 183 (1989).

16. B.C. Dems, Ph.D. Thesis, Cornell University (1990).

17. C.D. Child, Phys. Rev., 32, 492 (1911).

18. I. Langmuir, Phys. Rev., 2, 450 (1913).

19. B. Chapman, "Glow Discharge Processes," Wiley, New York (1981), p. 110.

Appendix

Laser Interferometer Thermometer Calibration

A soda-lime (plate) glass specimen with dimensions 1.0 cm x 1.0 cm x 0.102 cm thick (Evaporated Metal Films Inc., Ithaca, NY) was calibrated for use as a substrate thermometer. The plate glass specimen was bonded to the reflective side of a 1.5 cm x 1.5 cm piece of silicon wafer by applying a thin coat of colloidal silver paint in between. The backside of the silicon wafer was in turn bonded to a programmable hot stage (Mettler, Model FP-5) in the same way. The hot stage temperature was ramped from an initial temperature of 30.0°C to a final temperature of 200°C at a constant rate of 10.0°C per minute. The resulting interferogram is shown in figure A.1.

Temperature gradients within the plate glass-silicon specimen were neglected based on the following physical arguments. Assuming a mass density, heat capacity, and initial thickness of 2.50 g/cm^3, 0.753 J/g-°C, and 0.10 cm, respectively, an external heat flux on the order of 3.2×10^{-2} $Watts/cm^2$ is required to heat a plate glass specimen at a rate of 10.0°C/min (heating rates during RIE range from 5 to 40°C/min). On the other hand, thermal conductive heat fluxes <u>within</u> the glass specimen, estimated from $k\Delta T/d_o$ for $k = 7.53 \times 10^{-3}$ Watts/cm-°C and $\Delta T = 10$°C, are about 7.5×10^{-1} $Watts/cm^2$, or an order of magnitude greater than the heat flux from the hot stage. Therefore, thermal gradients within the specimen were negligible during both the calibration and RIE processing. The negligible thermal gradient condition was confirmed experimentally by observing the quick response (no time lag) of the reflected intensity signal as the heating rate was cycled randomly between 10°C/min and 0°C/min (i.e. constant temperature).

Referring to figure A.1, a total of ten interference fringes is obtained. This corresponds to a ΔT_p = 170°C/10 = 17°C per fringe. A more exact value of ΔT_p was determined from the average temporal period of reflectance oscillation (=99.3 ± 3.2sec). This corresponded to a ΔT_p of (1/99.3sec) x (10.0°C/min) x (min/60sec) = 16.6°C per fringe ±3%. The constant period of oscillation throughout the run implies a nearly constant mass density and heat capacity for the temperature range studied.

Similar, but thicker, plate glass specimens (d_o > 0.102 cm) could not be calibrated due to limitations of the hot stage. Calibration constants for glass specimens with d_o > 0.102 cm were estimated by assuming the same coefficient of thermal expansion and mass density for all specimens, and scaling ΔT_p with thickness (Table A.1). This was expected to be alright since all specimens were from the same stock.

Table A.1. Calibration constant† ΔT_p for plate glass specimens.

Plate Glass Thickness (cm)	ΔT_p (°C per fringe)
0.102	16.6 ± 0.5 (± 3%)
0.157	10.7 ± 0.3
0.236	7.1 ± 0.2

† Obtained by scaling 0.102cm results with glass thickness

FIGURE CAPTIONS

Figure 1: Laser interferometry of plate-glass substrate during RIE.

Figure 2: Interferograms of plate-glass substrates generated by heating and cooling in argon and oxygen RIE. Specimen Dimensions: 0.106 cm x 5.0 cm x 5.0 cm. RIE conditions: 0.50 W/cm^2, 35 mTorr, 20 SCCM, 550-575 Vdc.

Figure 3: Plate-glass temperature versus time plots generated from the interferograms in figure 2.

Figure 4: Argon and oxygen ion energy fluxes as a function of time. Plots were generated from data in figures 2 and 3.

Figure 5: Plate-glass temperature versus time at various rf power densities. Argon (top) and oxygen (bottom). RIE conditions: 35 mTorr, 20 SCCM; Specimen dimensions: 0.237 cm x 5.0 cm x 5.0 cm.

Figure 6: Steady-state temperature of 0.237 cm thick plate-glass versus incident rf power density in argon and oxygen. Conditions were the same as in figure 5.

Figure 7: Ion energy flux versus incident rf power density. RIE conditions were the same as in figure 7.

Figure 8: Percent of rf power delivered to cathode versus nominal incident rf power density.

Figure 9: Oxygen ion energy flux versus pressure at various rf power densities using a quartz cathode. Plate-glass specimen dimensions: 0.237 cm x 5.0 cm x 5.0 cm.

Figure 10: Oxygen RIE rate of PMMA (top) and PS (bottom) versus pressure at various rf power density. Gas flow rate: 20 SCCM.

Figure 11: Oxygen RIE rate for PMMA and PS versus measured ion energy flux. The data are the same as in figures 5.10 and 5.11. The open squares are data obtained by Visser and de Vries during oxygen RIE rate of novolac resist [20].

Figure A.1: Calibration interferogram of plate glass (heating rate = 10.0°C/min).

Figure 1: Laser interferometry of plate-glass substrate during RIE.

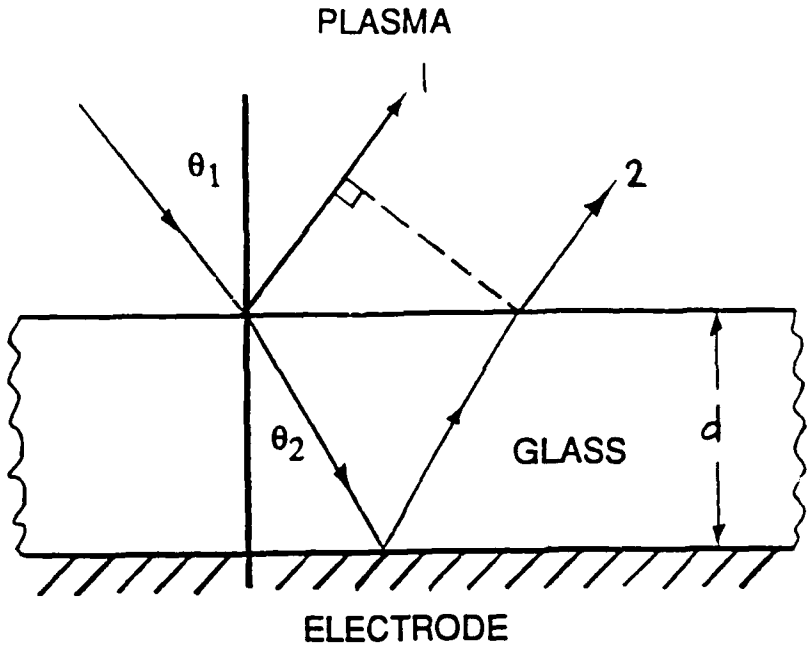

Figure 2: Interferograms of plate-glass substrates generated by heating and cooling in argon and oxygen RIE. Specimen Dimensions: 0.106 cm x 5.0 cm x 5.0 cm. RIE conditions: 0.50 W/cm^2, 35 mTorr, 20 SCCM, 550-575 Vdc.

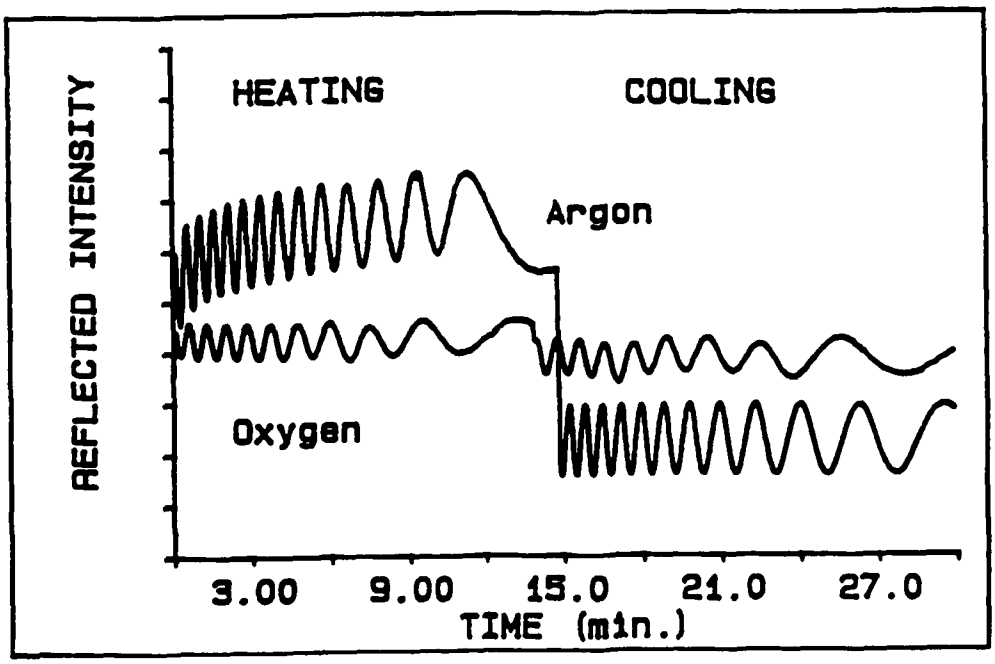

Figure 3: Plate-glass temperature versus time plots generated from the interferograms in figure 2.

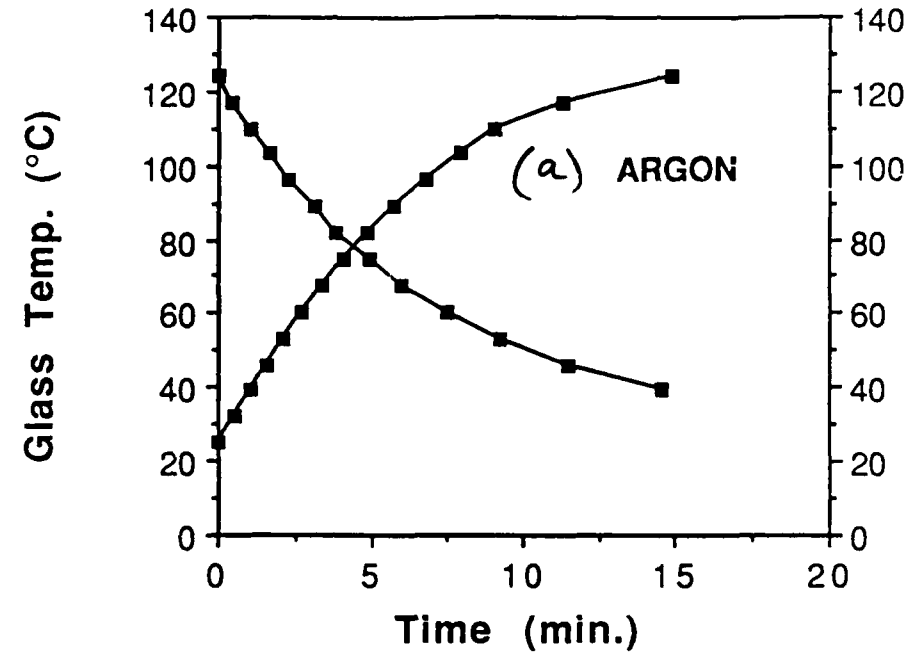

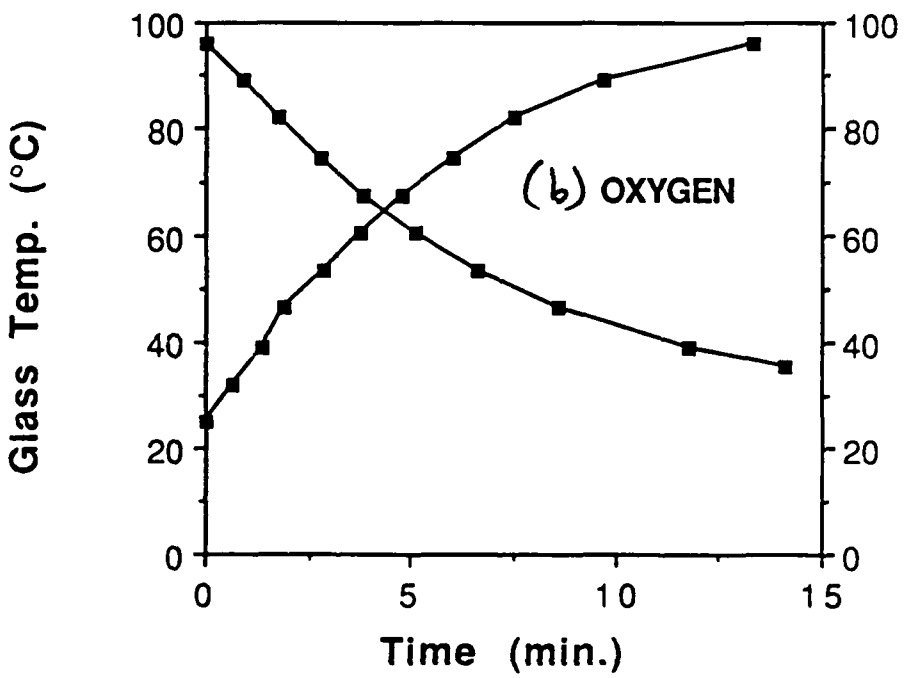

Figure 4: Argon and oxygen ion energy fluxes as a function of time. Plots were generated from data in figures 2 and 3.

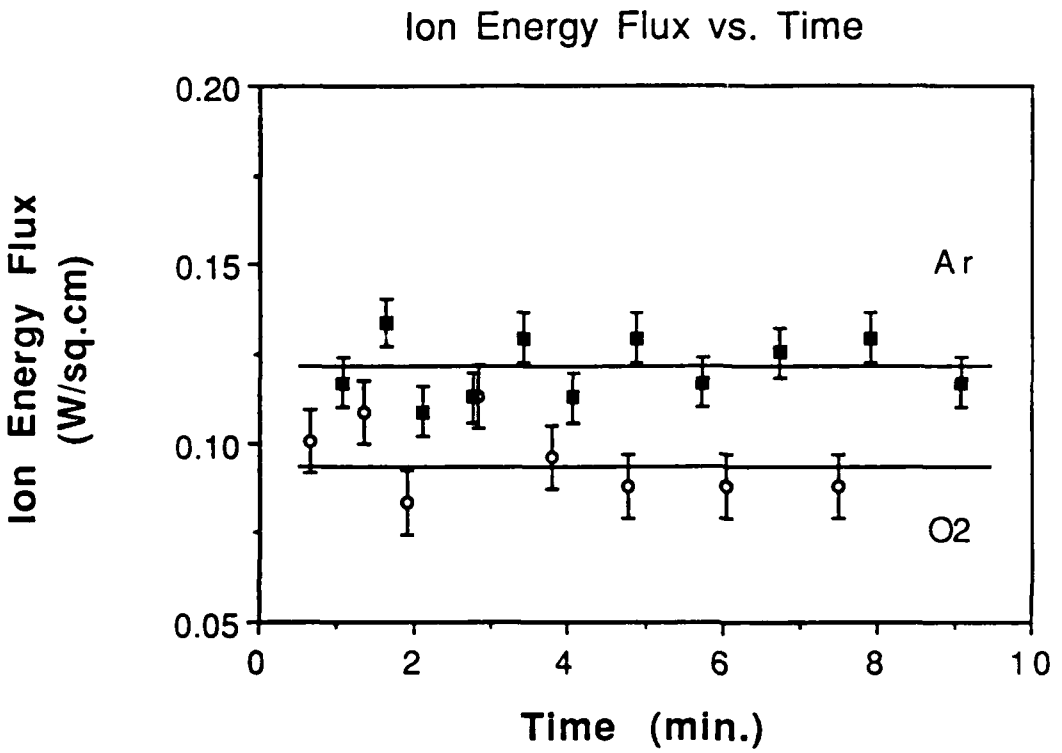

Figure 5: Plate-glass temperature versus time at various rf power densities. Argon (top) and oxygen (bottom). RIE conditions: 35 mTorr, 20 SCCM; Specimen dimensions: 0.237 cm x 5.0 cm x 5.0 cm.

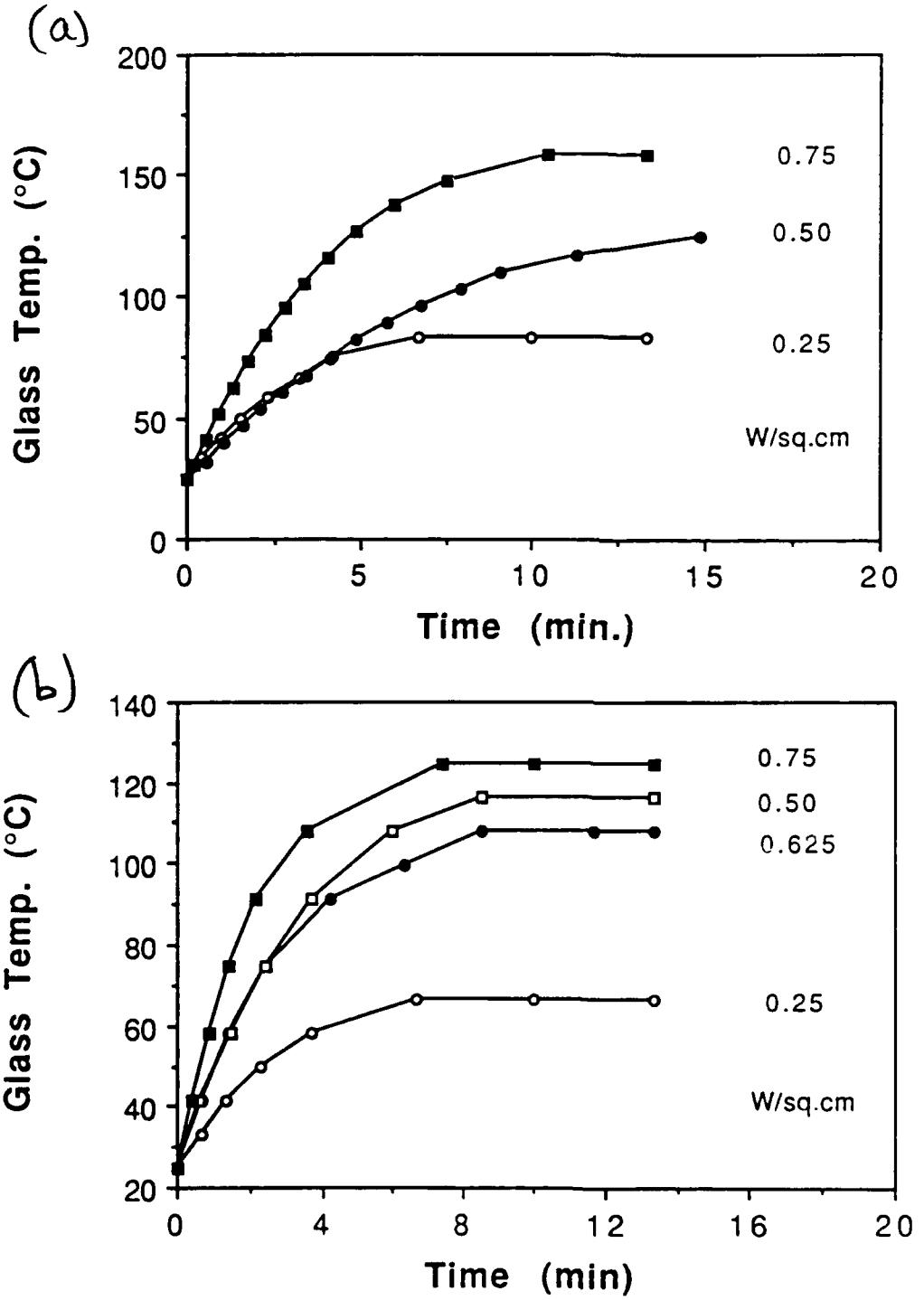

Figure 6: Steady-state temperature of 0.237 cm thick plate-glass versus incident rf power density in argon and oxygen. Conditions were the same as in figure 5.

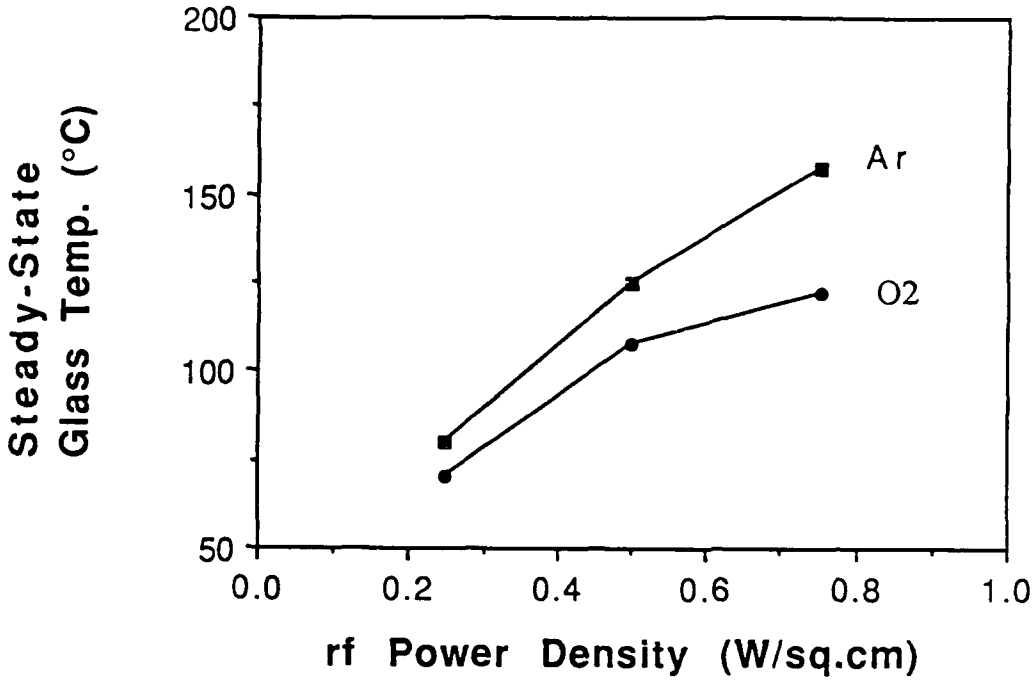

Figure 7: Ion energy flux versus incident rf power density. RIE conditions were the same as in figure 7.

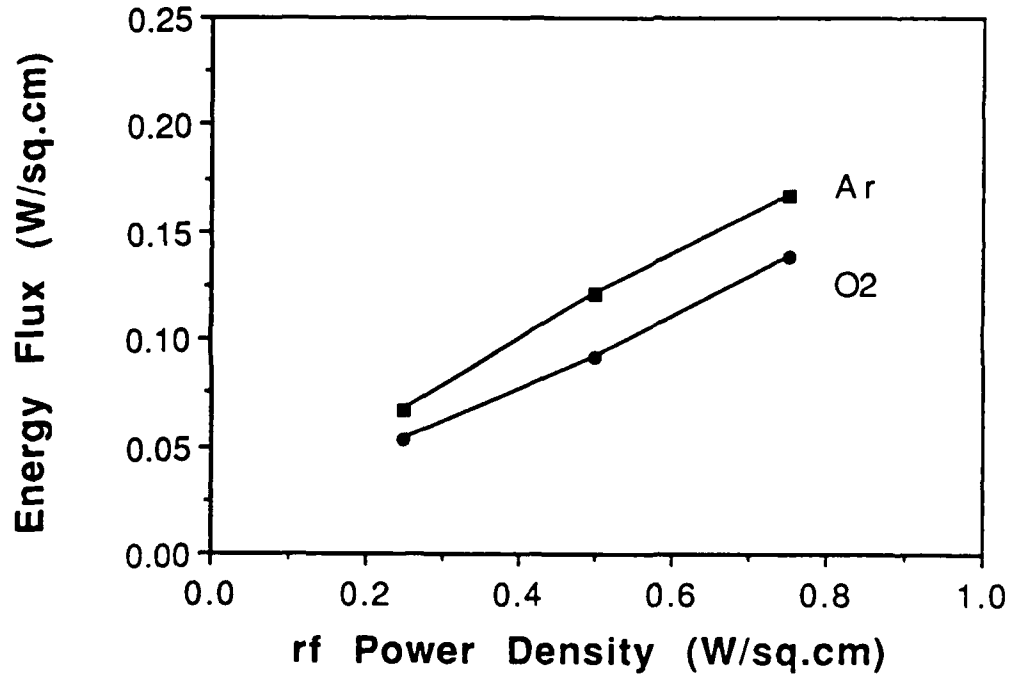

Figure 8: Percent of rf power delivered to cathode versus nominal incident rf power density.

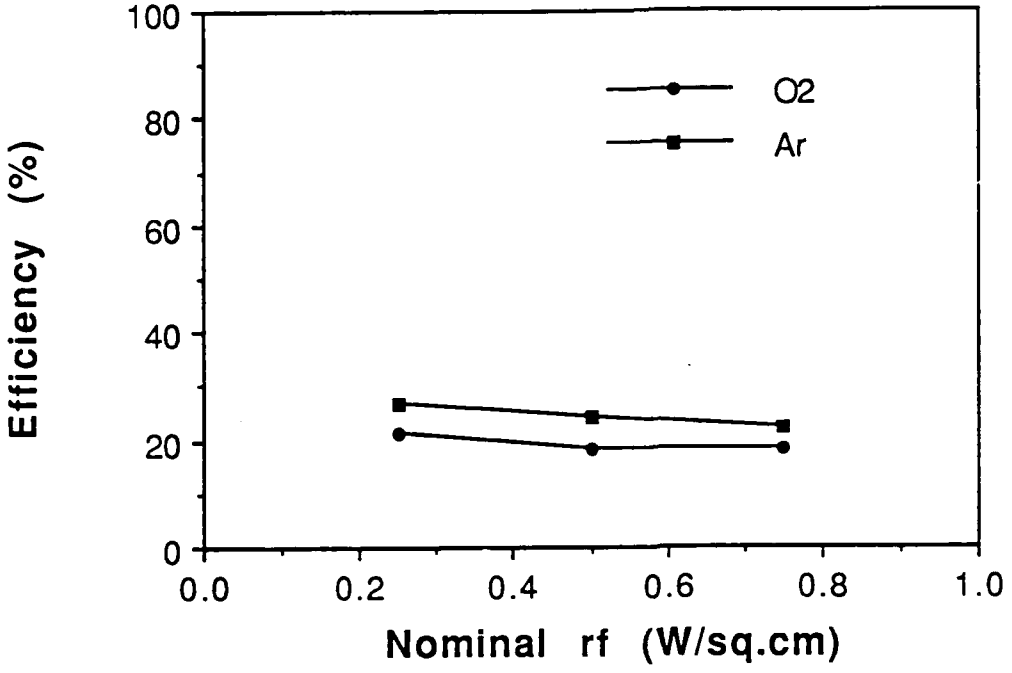

Figure 9: Oxygen ion energy flux versus pressure at various rf power densities using a quartz cathode. Plate-glass specimen dimensions: 0.237 cm x 5.0 cm x 5.0 cm.

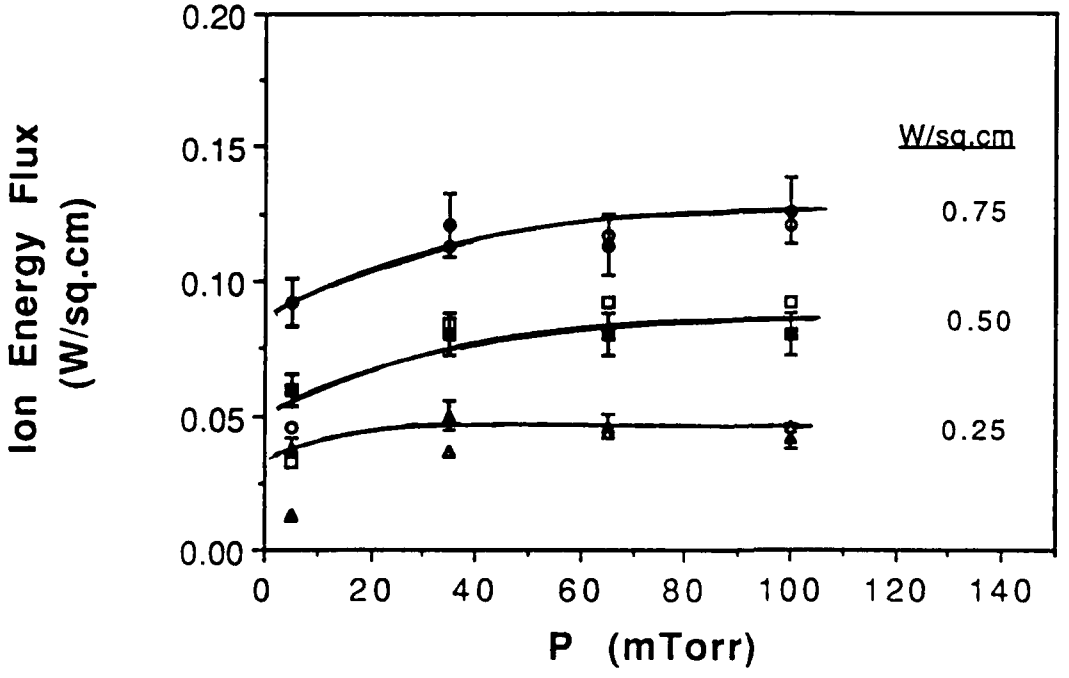

Figure 10: Oxygen RIE rate of PMMA (top) and PS (bottom) versus pressure at various rf power density Gas flow rate: 20 SCCM.

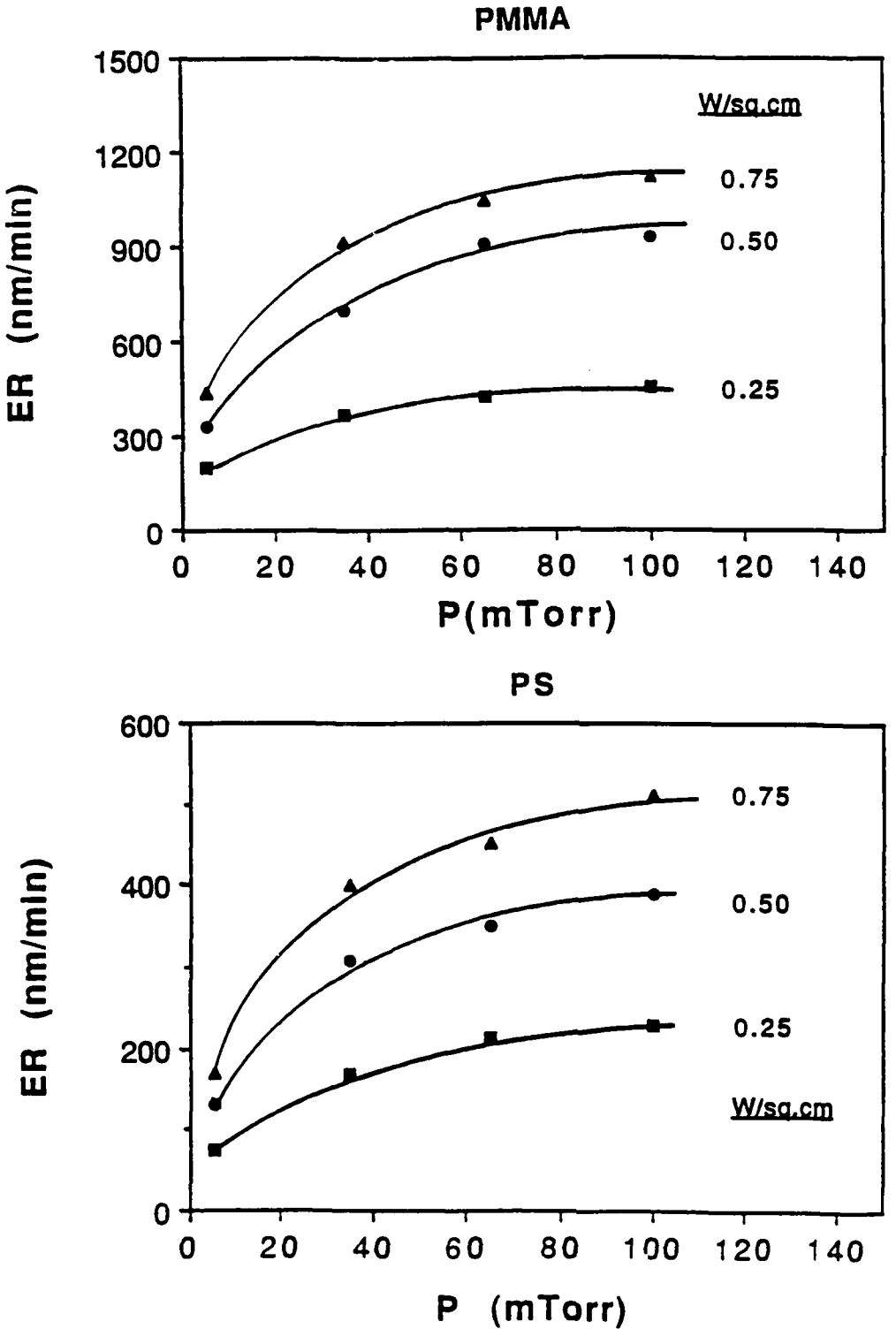

Figure 11: Oxygen RIE rate for PMMA and PS versus measured ion energy flux. The data are the same as in figures 5.10 and 5.11. The open squares are data obtained by Visser and de Vries during oxygen RIE rate of novolac resist [20].

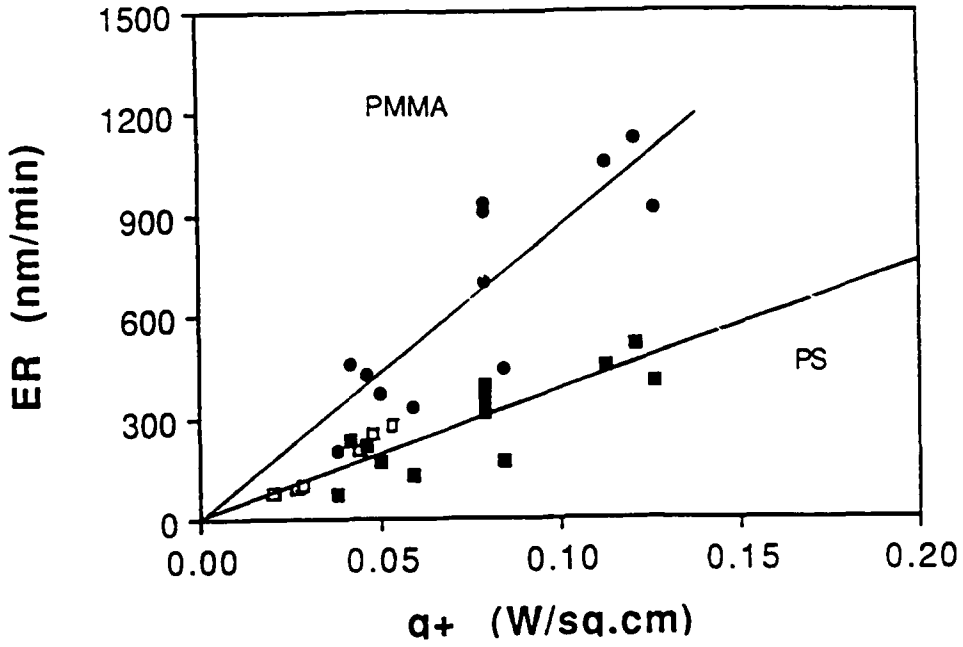

Figure A.1: Calibration interferogram of plate glass (heating rate = 10.0°C/min).

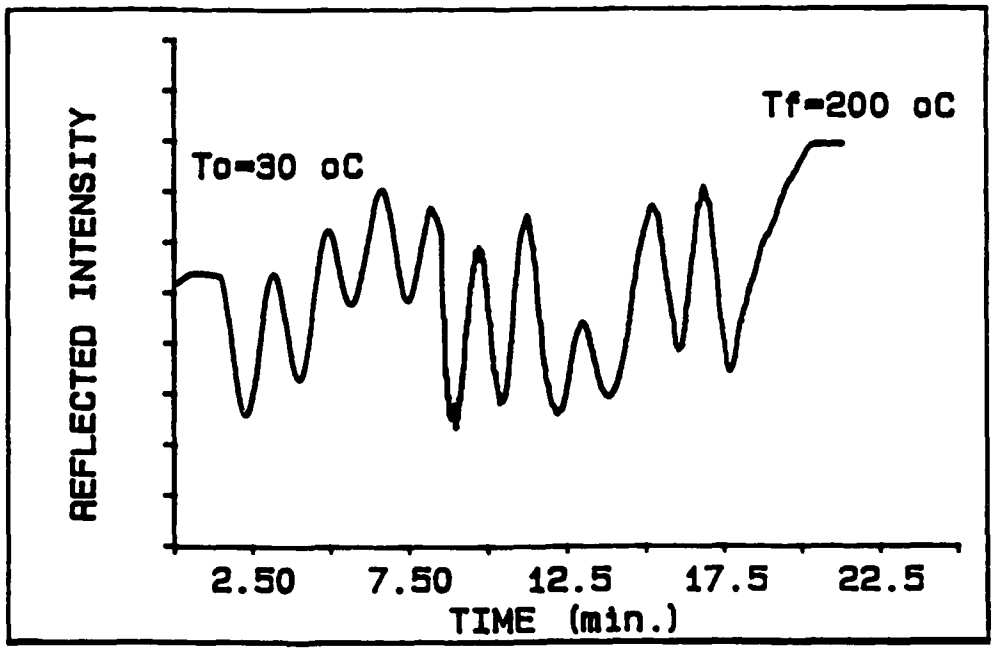

TECHNICAL REPORT DISTRIBUTION LIST - GENERAL

Office of Naval Research (2)
Chemistry Division, Code 1113
800 North Quincy Street
Arlington, Virginia 22217-5000

Dr. Robert Green, Director (1)
Chemistry Division, Code 385
Naval Weapons Center
China Lake, CA 93555-6001

Commanding Officer (1)
Naval Weapons Support Center
Dr. Bernard E. Douda
Crane, Indiana 47522-5050

Chief of Naval Research (1)
Special Assistant for Marine Corps Matters
Code 00MC
800 North Quincy Street
Arlington, VA 22217-5000

Dr. Richard W. Drisko (1)
Naval Civil Engineering Laboratory
Code L52
Port Hueneme, CA 93043

Dr. Bernadette Eichinger (1)
Naval Ship Systems Engineering Station
Code 053
Philadelphia Naval Base
Philadelphia, PA 19112

David Taylor Research Center (1)
Dr. Eugene C. Fischer
Annapolis, MD 21402-5067

Dr. Sachio Yamamoto (1)
Naval Ocean Systems Center
Code 52
San Diego, CA 92152-5000

Dr. James S. Murday (1)
Chemistry Division, Code 6100
Naval Research Laboratory
Washington, D.C. 20375-5000

Dr. Harold H. Singerman (1)
David Taylor Research Center
Code 283
Annapolis, MD 21402-5067

Defense Technical Information Center (2)
Building 5, Cameron Station
Alexandria, VA 22314